Complete and incomplete fusion reactions in the $^{16}O+^{169}Tm$ system: Excitation functions and recoil range distributions

Manoj Kumar Sharma,[1] Unnati,[1] B. K. Sharma,[1] B. P. Singh,[1] H. D. Bhardwaj,[2] Rakesh Kumar,[3] K. S. Golda,[3] and R. Prasad[1]

[1]*Department of Physics, Aligarh Muslim University, Aligarh-202002, (U.P.), India*

[2]*Department of Physics, DSN College, Unnao-209801, (U.P.), India*

[3]*Nuclear Science Centre, New Delhi, India*

(Received 3 September 2003; published 11 October 2004)

With the view to study complete and incomplete fusion in heavy ion induced reactions, experiments have been carried out for measuring excitation functions for several reactions in the system $^{16}O+^{169}Tm$ at energies near the Coulomb barrier to well above it, using an activation technique. The measured excitation functions have been compared with those calculated theoretically using three different computer codes viz., ALICE-91, CASCADE and PACE2. The enhancement of experimentally measured cross sections for alpha emission channels over their theoretical prediction has been attributed to the fact that these residues are formed not only by complete fusion but also through incomplete fusion. In order to separate out the relative contributions of complete and incomplete fusion, the recoil range distributions of eight residues produced in the interaction of ^{16}O with ^{169}Tm at $\approx$87 MeV have been measured. The recoil range distributions indicate significant contributions from incomplete fusion at $\approx$87 MeV for some of the channels.

DOI: 10.1103/PhysRevC.70.044606 PACS number(s): 25.70.Jj

I. INTRODUCTION

During the last couple of years there has been a renewed interest in the study of incomplete fusion reactions in heavy ion (HI) interactions particularly with heavier target nuclei. It has been observed that at energies just above the Coulomb barrier, both the complete fusion (CF) and the incomplete fusion (ICF) may be the dominant reaction mechanisms. In CF reactions, the incident ion completely fuses with the target nucleus, forming an excited composite system, from which particles and/or γ-rays may be emitted. However, in case of ICF, the projectile is assumed to break up into the fragments (e.g., ^{16}O may break up into ^{12}C and an α-particle; two ^{8}Be fragments; an α-particle and ^{12}C), one of which fuses with the target nucleus while the rest of it moves in the forward direction with almost same velocity as that of incident ion. The excited system formed as a result of the fusion of one of the fragments of the incident ion may also under go de-excitation by the emission of particles and/or gamma rays. Recent measurements of excitation functions (EFs) [1–4] for the production of large number of residues in HI reactions have indicated that ICF plays an important role in such reactions. However, the relative contributions of CF and ICF components, their dependence on energy, projectile-target combinations, etc. have not yet been fully explored and understood. Such measurements are still limited to a few systems only. As such, to have a better understanding of CF and ICF processes, more experimental data on EFs and recoil range distributions (RRDs) of the residues in HI reactions, covering a wide range of the periodic table and energy is required. It is possible to separate out the relative contributions of various ICF channels at energies near and just above the Coulomb barrier from the measurement of EFs and the RRD of evaporation residues. The measurement of RRD is based on the linear momentum transfer of the projectile to the target nucleus. In CF reactions, the linear momentum is completely transferred to the target nucleus, while in the case of ICF reactions, partial transfer of projectile momentum takes place. Most of the earlier studies of ICF reactions have been done at beam energies $>$10 MeV/nucleon using medium-mass targets. However, there are limited studies at lower beam energies with heavier targets ($A>150$). Further, when medium mass targets are used, it becomes difficult to distinguish the residues produced by CF and ICF mechanisms, as α-emission from the fused excited system is quite pronounced. However, if heavier targets are used, the emission of α-particles from the fused excited system is likely to be substantially reduced [5] due to the high Coulomb barrier. As a result, the emission of α-particles in ICF channels will give rise to heavy residues which have a very little contribution from CF channels. With a view to study CF and ICF in several projectile-target combinations, a program of precise measurement and analysis of EFs and RRD has been undertaken [6–10]. In the present work, excitation functions for eight reactions in the system $^{16}O+^{169}Tm$, in the energy range $\approx$71–95 MeV and recoil range distributions of the residues in the Al-catcher foils at $\approx$87 MeV beam energy have been measured, using the activation technique. The measured EFs have been compared with theoretical calculations done using three different codes viz., ALICE-91 [11], CASCADE [12], and PACE2 [13]. To the best of our knowledge these EFs as well as the RRDs have been measured for the first time. The analysis of EFs and RRDs have clearly indicated that ICF is a dominant mode of reaction mechanism at these energies. The experimental details are discussed in Sec. II of the paper. The analysis of excitation functions and recoil range distribution are given in Secs. III and IV of the paper, respectively.

II. EXPERIMENTAL DETAILS

Excitation functions

The experiments have been carried out using the 15 UD Pelletron accelerator facility of the Nuclear Science Center (NSC), New Delhi, India. Details of sample preparation, irradiation, post-irradiation analysis, etc., are given in the following sections.

1. Sample preparation

The samples of natural ^{169}Tm were prepared by the vacuum evaporation technique. The thickness of each target was determined by the α transmission method which is based on the measurement of the energy lost by 5.485 MeV α particles obtained from an ^{241}Am source, while passing through the sample. The thicknesses of the ^{169}Tm deposited on Al-foils ($\approx$1.5 mg/cm^2) were $\approx$0.6 mg/cm^2. The samples were cut into size of 1.2×1.2 cm^2 each and were pasted on rectangular Al-holders having concentric holes of 1.0 cm diameter. The Al-holders were used for rapid heat dissipation. The thick Al-backing of ^{169}Tm samples served both as an energy degrader as well as a catcher, so that recoiling residues may be trapped in catcher thickness.

2. Irradiation

The irradiations were carried out in the General Purpose Scattering Chamber (GPSC) of 1.5 m diameter having an in-vacuum transfer facility at the Pelletron accelerator facility of NSC, New Delhi, India. Two stacks containing four ^{169}Tm samples each were irradiated by an $^{16}O^{7+}$ beam at $\approx$92 and $\approx$95 MeV, respectively. The beam current was $\approx$30–50 nA. The targets of ^{169}Tm backed by an Al-catcher were placed normal to the beam direction so that the recoiling nuclei coming out of the target may be trapped in the catcher foil. Keeping in view the half lives of interest, the irradiations were carried out for $\approx$8 hours duration each. The delay time between the stop of irradiation and the beginning of counting was minimized using an in-vacuum transfer of samples. The total charge collected in the Faraday cup has been used to calculate the flux of the beam.

3. Post-irradiation analysis

The stack of samples after irradiation was taken out from the scattering chamber using an in-vacuum transfer facility. The activities induced in various samples were recorded by counting the target and catcher foils together using a HPGe γ-ray spectrometer coupled to the PC based multichannel analyzer. Software FREEDOM [14] has been used for recording and analysis of the data. The HPGe detector (resolution $\approx$2 keV for a 1.33 MeV γ-ray of ^{60}Co) was precalibrated both for energy and efficiency using various standard γ sources like ^{22}Na, ^{54}Mn, ^{57,60}Co, ^{133}Ba, ^{137}Cs, and ^{152}Eu. The geometry dependent efficiency of the HPGe detector for various source-detector distances was determined using a ^{152}Eu source. A typical γ-ray spectrum of an irradiated ^{169}Tm sample at 92 MeV is shown in Fig. 1. The various peaks in observed γ-ray spectra were assigned to different residues on the basis of their characteristic energy and

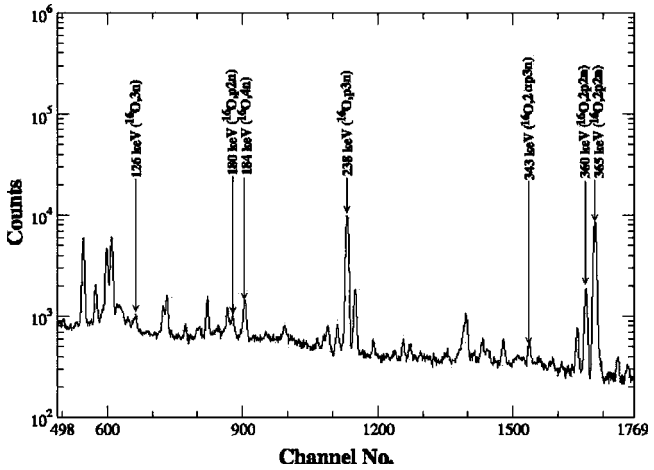

FIG. 1. A typical observed γ-ray spectrum for the $^{16}O+^{169}$Tm system at 92 MeV.

measured half-lives. The data for the half-life was fitted using the software ORIGIN. A list of reactions, energy of identified γ-rays and their branching ratios are given in Table I. The intensities of the characteristic γ-rays were used to compute the reaction cross sections using the formulation [9]

$$\sigma_r(E) = \frac{A\lambda\ \exp(\lambda t_2)}{N_o\phi\theta K(G\varepsilon)[1-\exp(-\lambda t_1)][1-\exp(-\lambda t_3)]}, \tag{1}$$

where A is the observed counts during the accumulation time t_3 of the induced activity of decay constant λ, N_0 is the number of target nuclei irradiated for time t_1 with a particle beam of flux ϕ, t_2 is the time lapse between the stop of irradiation and the start of counting, θ is the branching ratio of the characteristic γ ray and $G\varepsilon$ is the geometry dependent

TABLE I. List of reactions, energy of identified γ-rays and their branching ratios.

S. No.	Reaction	E_γ (keV)	Abundance (%)
1.	^{169}Tm(^{16}O,3n)^{182}Ir	126.9	34.4
		273.1,764.2	43,5.6
		891.1,912.2	5.7,8.7
2.	^{169}Tm(^{16}O,4n)^{181}Ir	107.6,123.5	15.2,4.3
		184.6,227.0	4.3,8.9
		231.6,318.9	4.6,7.0
3.	^{169}Tm(^{16}O,$p2n$)^{182}Os	180.22	34.7
		263.29	6.6
4.	^{169}Tm(^{16}O,$p3n$)^{181g}Os	238.68	44
		826.74	20.2
5.	^{169}Tm(^{16}O,$2p2n$)^{181}Re	360.7	20
		365.59	57.0
6.	^{169}Tm(^{16}O,$\alpha3n$)^{178}Re	237.19	45
7.	^{169}Tm(^{16}O,$2\alpha pn$)^{175}Hf	343.4	87
8.	^{169}Tm(^{16}O,$3\alpha n$)^{172}Lu	1093.6	63.5

TABLE II. The experimentally measured cross sections.

Lab energy (MeV)	$\sigma(^{182}\mathrm{Ir})$ (mb)	$\sigma(^{181}\mathrm{Ir})$ (mb)	$\sigma_{cum}(^{182}\mathrm{Os})$ (mb)	$\sigma_{ind}(^{182}\mathrm{Os})$ (mb)	$\sigma_{cum}(^{181}\mathrm{Os})$ (mb)	$\sigma(^{181}\mathrm{Re})$ (mb)	$\sigma(^{178}\mathrm{Re})$ (mb)	$\sigma(^{175}\mathrm{Hf})$ (mb)	$\sigma(^{172}\mathrm{Lu})$ (mb)
71.7±1.0	3.28±0.7	—	4.58±1.4	1.26±0.6	2.72±0.4	2.66±0.7	—	—	—
74.9±0.9	42.30±7.2	28.47±12.5	82.77±10.0	39.98±5.1	4.81±1.2	5.35±0.7	—	—	—
78.7±0.9	59.86±13.9	110.00±15.65	139.41±22.9	78.85±13.8	32.81±4.3	137.37±28.7	1.74±0.2	—	14.93±2.1
82.0±0.8	86.43±14.8	170.47±28.4	155.6±20.7	68.15±8.3	129.0±16.3	391.49±83.0	5.2±0.8	—	20.58±2.6
85.8±0.8	47.64±7.7	250.16±67.7	107.46±14.4	59.28±7.5	198.02±23.3	594.02±90.6	9.02±1.2	0.57±0.1	31.32±3.9
88.9±1.0	35.23±3.9	316.79±34.8	71.50±9.9	35.84±6.2	250.92±31.1	607.94±86.7	27.34±5.3	2.53±0.4	30.27±3.7
91.6±0.4	13.77±3.2	229.84±39.6	29.37±4.1	15.45±4.4	153.8±17.8	526.23±78.6	32.14±3.7	2.96±0.5	28.39±3.1
94.6±0.4	8.47±1.4	183.89±27.2	18.42±3.7	9.85±2.7	173.1±22.8	441.99±66.9	34.31±5.5	4.62±0.6	28.1±3.3

efficiency of the detector. The factor $[1-\exp(-\lambda t_1)]$ takes care of the decay of evaporation residue during the irradiation and is typically known as the saturation correction. The correction for the decay of the induced activity due to the delay between the stop of irradiation and the start of counting and during the data accumulation is taken into account via the factors $\exp(\lambda t_2)$ and $[1-\exp(-\lambda t_3)]$, respectively. $K=[1-\exp(-\mu d)/\mu d]$ is the correction for the self absorption of the γ radiations in the sample thickness itself, where d is the thickness of the sample and μ is the γ ray absorption coefficient.

Excitation functions for reactions $^{169}\mathrm{Tm}(^{16}\mathrm{O},3n)^{182}\mathrm{Ir}$, $^{169}\mathrm{Tm}(^{16}\mathrm{O},4n)^{181}\mathrm{Ir}$, $^{169}\mathrm{Tm}(^{16}\mathrm{O},p2n)^{182}\mathrm{Os}$, $^{169}\mathrm{Tm}(^{16}\mathrm{O},p3n)^{181}\mathrm{Os}$, $^{169}\mathrm{Tm}(^{16}\mathrm{O},2p2n)^{181}\mathrm{Re}$, $^{169}\mathrm{Tm}(^{16}\mathrm{O},\alpha 3n)^{178}\mathrm{Re}$, $^{169}\mathrm{Tm}(^{16}\mathrm{O},2\alpha pn)^{175}\mathrm{Hf}$, and $^{169}\mathrm{Tm}(^{16}\mathrm{O},3\alpha n)^{172}\mathrm{Lu}$ have been measured in the energy range $\approx 71-95$ MeV. The measured cross sections are tabulated in Table II. It may be pointed out that reactions $^{169}\mathrm{Tm}(^{16}\mathrm{O},3n)^{182}\mathrm{Ir}$, $^{169}\mathrm{Tm}(^{16}\mathrm{O},4n)^{181}\mathrm{Ir}$, $^{169}\mathrm{Tm}(\mathrm{O},p2n)^{182}\mathrm{Os}$, and $^{169}\mathrm{Tm}(^{16}\mathrm{O},p3n)^{181}\mathrm{Os}$ may be populated only via CF. However, the reactions $^{169}\mathrm{Tm}(^{16}\mathrm{O},2p2n)^{181}\mathrm{Re}$, $^{169}\mathrm{Tm}(^{16}\mathrm{O},\alpha 3n)^{178}\mathrm{Re}$, $^{169}\mathrm{Tm}(^{16}\mathrm{O},2\alpha pn)^{175}\mathrm{Hf}$, and $^{169}\mathrm{Tm}(^{16}\mathrm{O},3\alpha n)^{172}\mathrm{Lu}$ may be populated not only by CF but also by ICF.

In the interaction of heavy ions with a target nucleus, some of the residues are produced directly (independent yield) while some of them are also produced in the decay of a higher charge isobar precursor (cumulative yield) nucleus through β^+ emission, and/or electron capture. For such cases, cumulative cross sections have been measured if the half-life of the precursor is considerably smaller than that of the residue, by analyzing the induced activities at times greater than about eight to ten half-lives of the precursor. The cumulative cross section of a given residue is the sum of (i) its independent production cross section and (ii) the cross section for the independent production of its precursor multiplied by a numerical coefficient which depends on the branching ratio for precursor decay to residue and the half-lives of the precursor and the residue. In such cases, the analysis given by Cavinato *et al.* [15] has been used to separate the contribution from precursor decay.

This has been done for the residue ^{182}Os, which may be formed via the reaction $^{169}\mathrm{Tm}(^{16}\mathrm{O},p2n)$ and may also be populated by the β^+ decay of higher charge isobar precursor ^{182}Ir produced via the reaction $^{169}\mathrm{Tm}(^{16}\mathrm{O},3n)$. As such, the measured activity of residue ^{182}Os has contributions from the precursor decay also. In the present work, the precursor contribution for the reaction $^{169}\mathrm{Tm}(^{16}\mathrm{O},p2n)$ has been separated and the cumulative as well as independent yields for this residue are given in Table II. The cross section for ^{181}Os given in Table II is cumulative, since this residue produced via reaction $^{169}\mathrm{Tm}(^{16}\mathrm{O},p3n)$ may also be populated through the β^+ decay of higher charge isobar pre-cursor ^{181}Ir produced via reaction $^{169}\mathrm{Tm}(^{16}\mathrm{O},4n)$. Since the β^+ decay of ^{181}Ir produces ^{181}Os (105 min) and ^{181m}Os (2.7 min) isotopes, the shorter half-life isotope could not be measured. As such, the precursor contribution for ^{181}Os could not be deduced.

III. ANALYSIS OF EXCITATION FUNCTIONS

The analysis of presently measured excitation functions has been performed using three different computer codes viz., ALICE-91 [11], CASCADE [12], and PACE2 [13]. In the following sections brief details of these codes along with their important parameters, etc. are discussed.

A. Analysis with Code ALICE-91

The code ALICE-91 [11] has been developed by Blann, to account for the equilibrium (CN) as well as pre-equilibrium (PE) emission in light and heavy ion induced reactions. The CN calculations in this code are performed using the Weisskopf-Ewing model [17], while the PE component is simulated using the Hybrid/Geometry Dependent Hybrid model [18]. In this code, the configuration of the initially excited number of particles and holes, also referred to as initial exciton number n_0, is the starting point in any particle induced nuclear reaction. In code ALICE-91, the intermediate states of the system are characterized by the excitation energy E and number n_p of excited particles and n_h of excited holes. Particles and holes are defined relative to the ground state of the nucleus and are called excitons. The initial configuration of the compound system defined by the exciton number $n_0=(n_p+n_h)$ is an important parameter of PE formalism. The code ALICE-91 calculates two-body nuclear transi-

tion rates using Pauli corrected free nucleon-nucleon scattering cross-section data. The actual mean free path (MFP) inside the nucleus may be quite different from the one calculated using free nucleon-nucleon scattering data. In order to compensate for this difference, a parameter COST is provided in the code ALICE-91. A value of COST greater than zero means a smaller value of actual MFP for nucleon-nucleon scattering inside a composite excited nucleus. As such, in this code the level density parameter a, the mean free path multiplier *COST* and initial exciton number n_0 are the important parameters. The level density parameter a largely affects the equilibrium component, while the initial exciton number n_0 and mean free path multiplier *COST* govern the pre-equilibrium component. The level density parameter a is calculated from the expression $a=A/K$, where A is the mass number of the residual nucleus and K is a parameter which can be varied to match the experimental data. In this work, a value of $K=22$ along with $n_0=16(8p+8n+0h)$ and $COST=2$, is found to reproduce the maximum magnitude of the experimental data satisfactorily, but energy dependence could not compare well. It may be clarified that when ALICE-91 calculations with above mentioned values of parameters were compared with their experimental counterparts, it was observed that the maxima of the measured EF's were at higher energies than those of the calculated EF's. This is expected, since in ALICE-91 calculations the angular momentum effects have not been taken into account. In HI induced reactions incident particle imparts relatively larger angular momentum to the composite system. If, in the last stages of nuclear de-excitation, higher angular momentum inhibits particle emission more than it does γ emission, then the peak of excitation function corresponding to the particle emission mode will be shifted to higher energies [19]. The effect is more pronounced in heavy ion (HI) reactions as compared to the light ion reactions, since the rotational energy is much greater in the case of HI reactions. An estimate of the possible shift due to angular momentum effects may be made from the nuclear rotational energy. For a rigid body, the rotational energy is given by $E_{rot}\approx(m/M)E_{lab}$. Here, m/M is the ratio of the projectile and the target nucleus masses and E_{lab} is the incident energy [19]. Since the angular momentum effects have not been considered in the Weisskopf-Ewing calculations of the present version of ALICE-91 code, it is desirable to shift the calculated excitation functions by the amount approximately equal to E_{rot} as calculated above. Similar shift has been observed in some earlier work also [6–8]. As an example, the calculated EFs with an energy shift equal to E_{rot} for reaction ^{169}Tm(^{16}O,3n)^{182}Ir is shown in Fig. 2. The unshifted calculated EF is also shown by a dotted curve in this figure for comparison. As such, in the present work, the calculated excitation functions for all the reactions have been shifted by E_{rot} on the energy scale as shown in Figs. 3 and 4 by dashed curves.

It may be mentioned that the nucleus ^{181}Ir is found to emit about 34 γ-rays, the relative intensities of which are given in the reference [16]. In the present measurements, the residual nucleus ^{181}Ir has been identified through γ-rays of energies 106.7 keV, 123.5 keV, 184.6 keV, 227 keV, 231.6 keV, and 318.9 keV. The absolute intensities of above mentioned γ-rays were calculated using relative intensity data of reference [16] and are given in Table I. It has been observed that the measured cross-section data agree with the theoretical calculations of code ALICE-91, as shown in Fig. 3(b). In Figs. 3(c) and 3(d) the experimentally measured and theoretically calculated EF's for the reactions ^{169}Tm(^{16}O,$p2n$)^{182}Os, and ^{169}Tm(^{16}O,$p3n$)^{181}Os are shown. The residue ^{182}Os may be populated independently as well as by the β^+ decay of its higher charge isobar precursor ^{182}Ir which may be formed via the reaction ^{169}Tm(^{16}O,3n). The open circles in Fig. 3(c) represent the cumulative yield for the production of the residue ^{182}Os. A brief detail of the method used for separating precursor contribution [15] is given here.

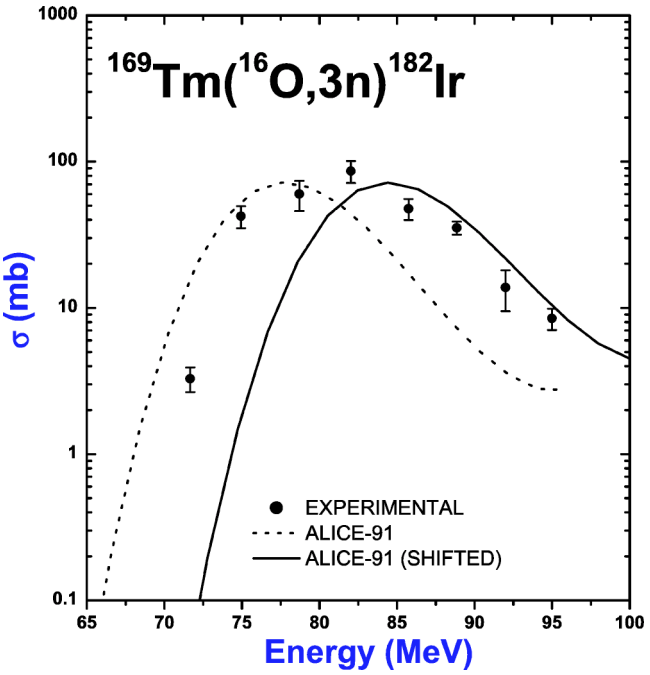

FIG. 2. The experimentally measured and theoretically calculated EFs using code ALICE-91. The calculated EF with an energy shift equal to E_{rot} is shown by a solid curve, while unshifted EF is represented by a dotted curve for comparison.

If a precursor P is formed with cross-section σ_P during the irradiation, and decays with half-life $T_{P1/2}$ and a branching ratio P_P, to a daughter nucleus D which is produced with cross-section σ_D during the irradiation and decays with half-life $T_{D1/2}$, the cumulative cross-section σ_C for the production of a daughter is given by

$$\sigma_C = \sigma_D + \sigma_P[T^{D_{1/2}}/(T^{D_{1/2}} - T^{P_{1/2}})]P_P. \quad (2)$$

Using the above formulation in the present case, the cumulative yield σ_{cum} and independent yields σ_{ind} are related by the equation

$$\sigma_{cum} = \sigma_{ind}(^{182}\mathrm{Os}) + 1.011709\sigma(^{182}\mathrm{Ir}). \quad (3)$$

The filled circles in Fig. 3(c) represent the observed independent yield of ^{182}Os as discussed above. As can be seen from Fig. 3(d), there is a discrepancy between the measured and calculated EF for the reaction ^{169}Tm(^{16}O,$p3n$)^{181}Os, which may be due to the contribution from its precursor decay. The observed enhancement, in Figs. 4(a) and 4(b), of measured

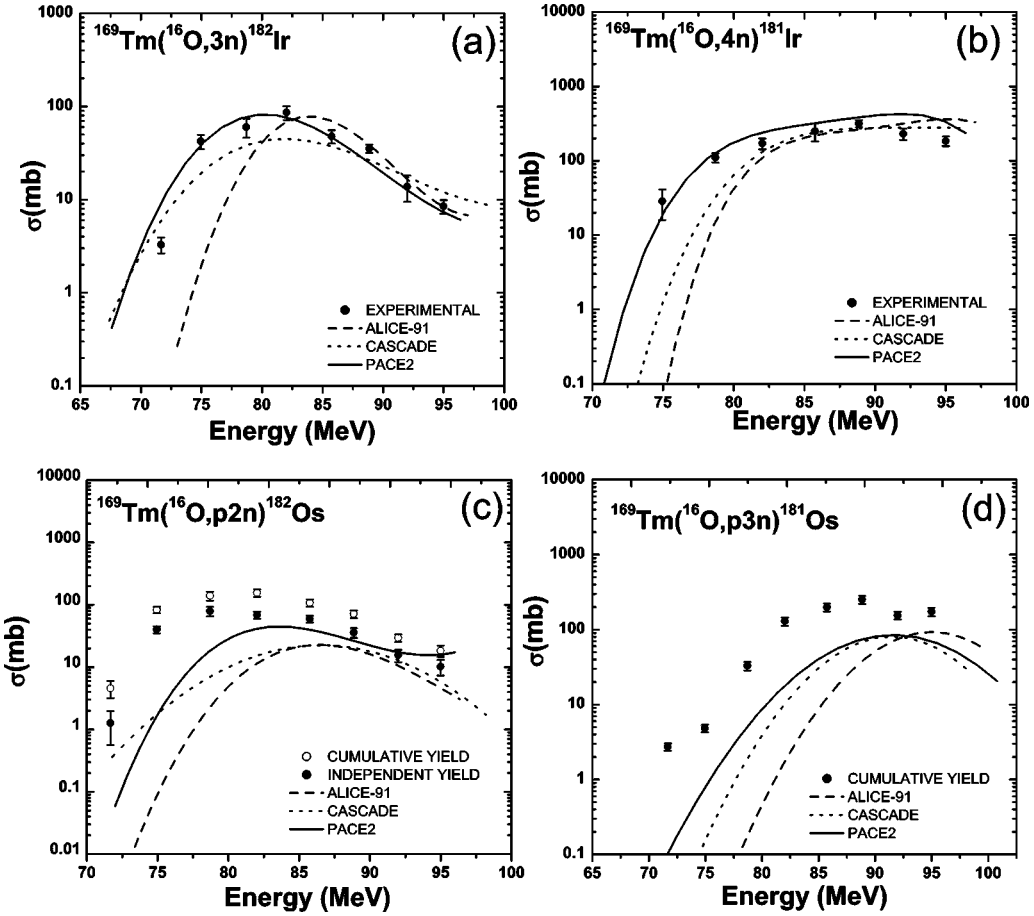

FIG. 3. The experimentally measured and theoretically calculated EF's using codes ALICE-91, CASCADE, and PACE2. In (c), the open circles represent the cumulative yield for the production of the residue ^{182}Os, while dark circles represent its independent yield.

EFs over their theoretically calculated values for the reactions ^{169}Tm(^{16}O,$2p2n$)^{181}Re and ^{169}Tm(^{16}O,$\alpha 3n$)^{178}Re may be attributed to the fact that these channels may be populated, not only by the CF of ^{16}O but may also have significant contributions from ICF (if ^{16}O breaks up into α, ^{8}Be and ^{12}C fragments). It may be pointed out that incomplete fusion is not taken into account in the ALICE-91 calculations. Further, the theoretical calculations for reactions ^{169}Tm(^{16}O,$2\alpha pn$)^{175}Hf and ^{169}Tm(^{16}O,$3\alpha n$)^{172}Lu are not shown in Figs. 4(c) and 4(d), since the calculated values of cross-sections for these cases are negligibly small ($<$0.01 mb). As such, it may be concluded that the major contribution to these reaction channels comes from the incomplete fusion.

B. Analysis with code CASCADE

The code CASCADE [12] is based on Hauser-Feshbach theory [20] and does not consider the possibility of incomplete fusion (ICF) and PE emission. In this code the level density parameter constant K and the ratio of actual moment of inertia to the rigid body moment of inertia of the excited system F_θ are the two important parameters which may be varied to match the experimental data. The Fermi-gas model is used in this code to calculate the level densities of the product nuclei. The transmission coefficients in these calculations are generated using the optical model potentials of Becchetti and Greenlees [21] for neutrons and protons and that of Satchler [22] for α-particles. In HI induced reactions of interest, the high angular momentum and excitation energy is expected to have considerable influence on the deexcitation cascade. Since in HI reactions an increase in excitation energy also increases the angular momentum, as such, the deformation of the nucleus due to the angular momentum effect may also be quite substantial. In these calculations, the deformation effects may be included by using an angular momentum dependent moment of inertia, which results into the deviation of the yrast line from that calculated assuming the nucleus to be a rigid sphere. The level density parameter a_f at the saddle point, which is obtained from the relation $a_f = A/D_{AF}$, where, A is the mass number of the compound nucleus and D_{AF} is a parameter, has also been found to influence the calculated EF's considerably. It has been observed that the parameter D_{AF} has a considerable influence on calculated EFs in the higher energy region. Further, a value of $K=14$, $D_{AF}=14$ with $F_\theta=0.85$ is found to give satisfactory agreement with experimental data. The CASCADE calculations in Figs. 3 and 4 are shown by dotted curves. As may be observed from these Figs. 3(a) and 3(b), the EFs for ^{169}Tm(^{16}O,$3n$)^{182}Ir and ^{169}Tm(^{16}O,$4n$)^{181}Ir reactions are in

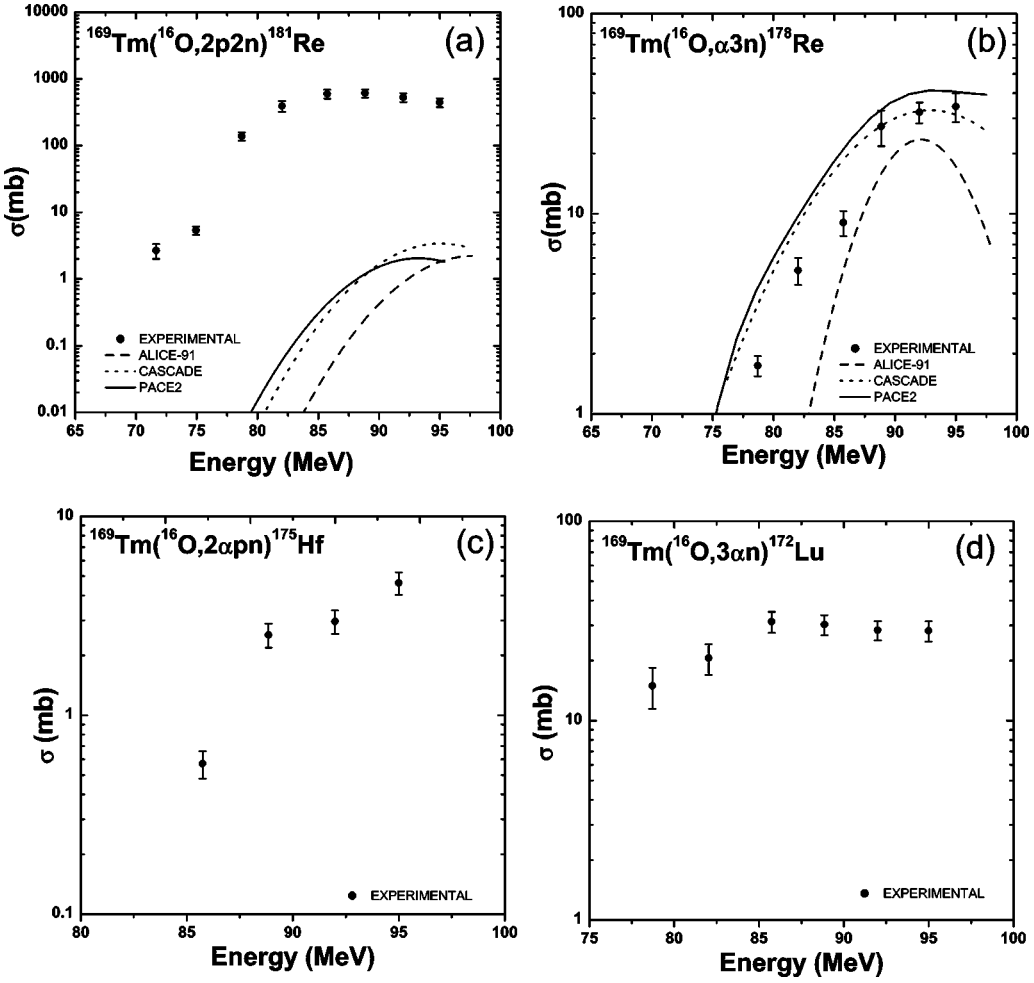

FIG. 4. The experimentally measured and theoretically calculated EFs using codes ALICE-91, CASCADE, and PACE2. In (c) and (d) calculated EFs are not shown as discussed in the text.

satisfactory agreement with theoretical calculations of code CASCADE. For reaction ^{169}Tm(^{16}O,$p2n$)^{182}Os, as can be seen from Fig. 3(c), the data peaks at a lower energy, and the predicted cross section is considerably larger than the calculation in the lower energy side. However, in case of reactions ^{169}Tm(^{16}O,$p3n$)^{181}Os [Fig. 3(d)], the discrepancy between the experimental and calculated excitation function may be due to the pre-cursor contribution from the residue ^{181}Ir. The reaction ^{169}Tm(^{16}O,$2p2n$)^{181}Re needs special mention. For this reaction, as shown in Fig. 4(a), theoretically calculated EFs do not match with the experimentally measured values. The theoretical calculations are much lower as compared to that of the experimentally measured EFs. This may be attributed to the fact that this channel may be populated not only by the CF of ^{16}O but also may have a significant contribution from ICF. Further, for the reactions ^{169}Tm(^{16}O,$2\alpha pn$)^{175}Hf, and ^{169}Tm(^{16}O,$3\alpha n$)^{172}Lu, the calculated values of EFs using code CASCADE are negligibly small (<0.01 mb) and could not be shown in Figs. 4(c) and 4(d). Since, the ICF has not been considered in CASCADE calculations, it may be concluded that the major contribution to these reaction channels comes from the incomplete fusion. Further, the EF for the residue ^{178}Re [Fig. 4(b)], which is expected to have a significant ICF component is reproduced well by this code which is quite surprising. In order to confirm the production of ^{178}Re via an ICF channel, the recoil range distribution for this residue has also been measured and details are is given in Sec. IV of this paper, which clearly indicates that ICF has a significant contribution for this channel.

C. Analysis with code PACE2

The code PACE2 [13] is based on a statistical approach. In this code the deexcitation of the CN is followed by a Monte Carlo procedure. The angular momentum projections are calculated at each stage of deexcitation which enables the determination of angular distribution of the emitted particles. In this code the level density parameter is one of the important parameters which may be varied to match the experimental data. In the present work, a value of level density parameter constant $K=16$ is taken for calculation. The calculated EFs for the reactions ^{169}Tm(^{16}O,$3n$)^{182}Ir, ^{169}Tm(^{16}O,$4n$)^{181}Ir, ^{169}Tm(O,$p2n$)^{182}Os, and ^{169}Tm(^{16}O,$p3n$)^{181}Os are shown in Figs. 3(a)–3(d). As can be seen from these figures that PACE2 calculations are in good agreement for the reactions

TABLE III. List of catcher-thicknesses used in RRD measurements.

S. No.	Thickness in $\mu g/cm^2$
1	16.8
2	19.6
3	27.4
4	27.8
5	28.6
6	29.5
7	30.2
8	30.6
9	31.3
10	31.9
12	32.1
13	33.2
14	33.9
15	37.1
16	39.9
17	44.2
18	46.1
19	47.0

^{169}Tm(^{16}O,3n)^{182}Ir and ^{169}Tm(^{16}O,4n)^{181}Ir, however, for reactions ^{169}Tm(O,p2n)^{182}Os and ^{169}Tm(^{16}O,p3n)^{181}Os, the discrepancy between experimental and calculated EFs may be due to their precursors contributions, as stated earlier. For reactions ^{169}Tm(O,2p2n)^{181}Re and ^{169}Tm(^{16}O,α3n)^{178}Re, the predictions of PACE2 are almost similar to that of code CASCADE as shown by solid curves in Figs. 4(a) and 4(b). In the case of reactions ^{169}Tm(^{16}O,2αpn)^{175}Hf and ^{169}Tm(^{16}O,3αn)^{172}Lu, the theoretical predictions are negligibly small, and hence are not shown in Figs. 4(c) and 4(d), while the measured cross sections are comparatively larger. This enhancement of the measured cross sections than their theoretical predictions may be associated with the ICF process.

IV. RECOIL RANGE DISTRIBUTIONS

The recoil range distributions (RRDs) for various radioactive residues produced in the interaction of the 86.6 MeV ^{16}O beam with the ^{169}Tm target nucleus have been measured. The target was mounted in the irradiation chamber with Al-backing facing the beam so that the catcher stack immediately followed the Thulium layer. The beam energy incident on front Al surface was 92 MeV. After an energy loss of $\approx$5 MeV in the Al thickness the incident beam energy was reduced to 86.6 MeV on the Tm material. A stack of 19 thin Al-catchers of thickness varying from $\approx$16–45 $\mu g/cm^2$ was used to trap the recoiling nuclide. The thicknesses of the Al-catcher foils used are given in Table III. The duration of irradiation was about 18 h with a beam fluence of $\approx$3500 μC. The activities induced in each catcher were followed off-line for about two weeks using a pre calibrated high resolution (2 keV for 1.33 MeV γ ray of ^{60}Co) HPGe detector of 100 c.c. active volume coupled to CAMAC based software FREEDOM [14] at NSC, New Delhi.

The cross-sections (σ) for a particular reaction product were computed using Eq. (1) as given in Sec. II. In order to obtain the yield distribution as a function of cumulative depth in the catcher stack, the cross section in each catcher was divided by its measured thickness. The resulting yields have been plotted in Figs. 5(a)–5(h) against cumulative catcher thickness to obtain the differential recoil range distributions. Solid curves guide the eye to the experimental data. As can be seen from the Figs. 5(a)–5(c), the recoil range distributions for ^{182}Ir and ^{181,182}Os isotopes produced via (^{16}O,3n), (^{16}O,p3n), and (^{16}O,p2n) channels, respectively, have a peak at only one value of cumulative catcher thickness $\approx$350 $\mu g/cm^2$. Here, RRD of Ir and Os isotopes are nearly Gaussian having peaks at a depth nearly corresponding to the expected recoil range of the compound system ^{185}Ir in aluminum, calculated using the classical approach and the stopping power tables of Northcliffe and Schilling [23]. It means that these products (Ir and Os) are formed by a complete fusion process only, followed by the evaporation of n and/or p. However, for reaction ^{169}Tm(^{16}O,2p2n)^{181}Re [Fig. 5(d)], the RRD has two peaks: one at a relatively lower value ($\approx$250 $\mu g/cm^2$) of cumulative catcher thickness and the other at $\approx$350 $\mu g/cm^2$, the same as in the case of complete fusion, respectively. In Fig. 5(d) the maxima at a larger value of cumulative thickness ($\approx$350 $\mu g/cm^2$) corresponds to the fraction of the residues produced through complete fusion, while the peak at relatively smaller range of cumulative catcher thickness ($\approx$250 $\mu g/cm^2$) may be attributed to the fact that the residue ^{181}Re is produced via incomplete fusion of ^{12}C, where the linear momentum transferred is expected to be less than that for the CF channel. In Fig. 5(e), it may be pointed out that the expected data points for the peak position of RRD at $\approx$350 $\mu g/cm^2$ for the residue ^{178}Re produced via the (^{16}O,α3n) reaction through CF could not be obtained due to the short half-life (13.3 m) of the residue. However, from the trend of RRD it may be observed that there may be two peaks: one corresponding to the ICF and the other due to the CF channel.

As expected, the observed recoil range distribution [Fig. 5(f)] for the ^{175}Hf isotope produced via ^{169}Tm(^{16}O,2αpn) reaction have three peaks at cumulative thicknesses $\approx$370 $\mu g/cm^2$, $\approx$260 $\mu g/cm^2$, and $\approx$150 $\mu g/cm^2$ corresponding to the residue ^{175}Hf produced via three different channels, i.e., (a) the complete fusion of ^{16}O with ^{169}Tm, forming the composite nucleus ^{185}Ir, followed by the emission of a proton, a neutron and two α-particles; (b) the incomplete fusion of ^{16}O, if it is assumed that ^{16}O breaks up into ^{12}C and; an α-particle and fragment ^{12}C fuses with ^{169}Tm, forming the composite nucleus ^{181}Re, followed by the emission of a proton, a neutron and α-particles; (c) the incomplete fusion of ^{16}O, assuming that ^{16}O breaks up into two ^{8}Be fragments and one of these fragments fuses with ^{169}Tm, forming the composite nucleus ^{177}Ta, followed by the emission of a proton, and a neutron. For the reactions

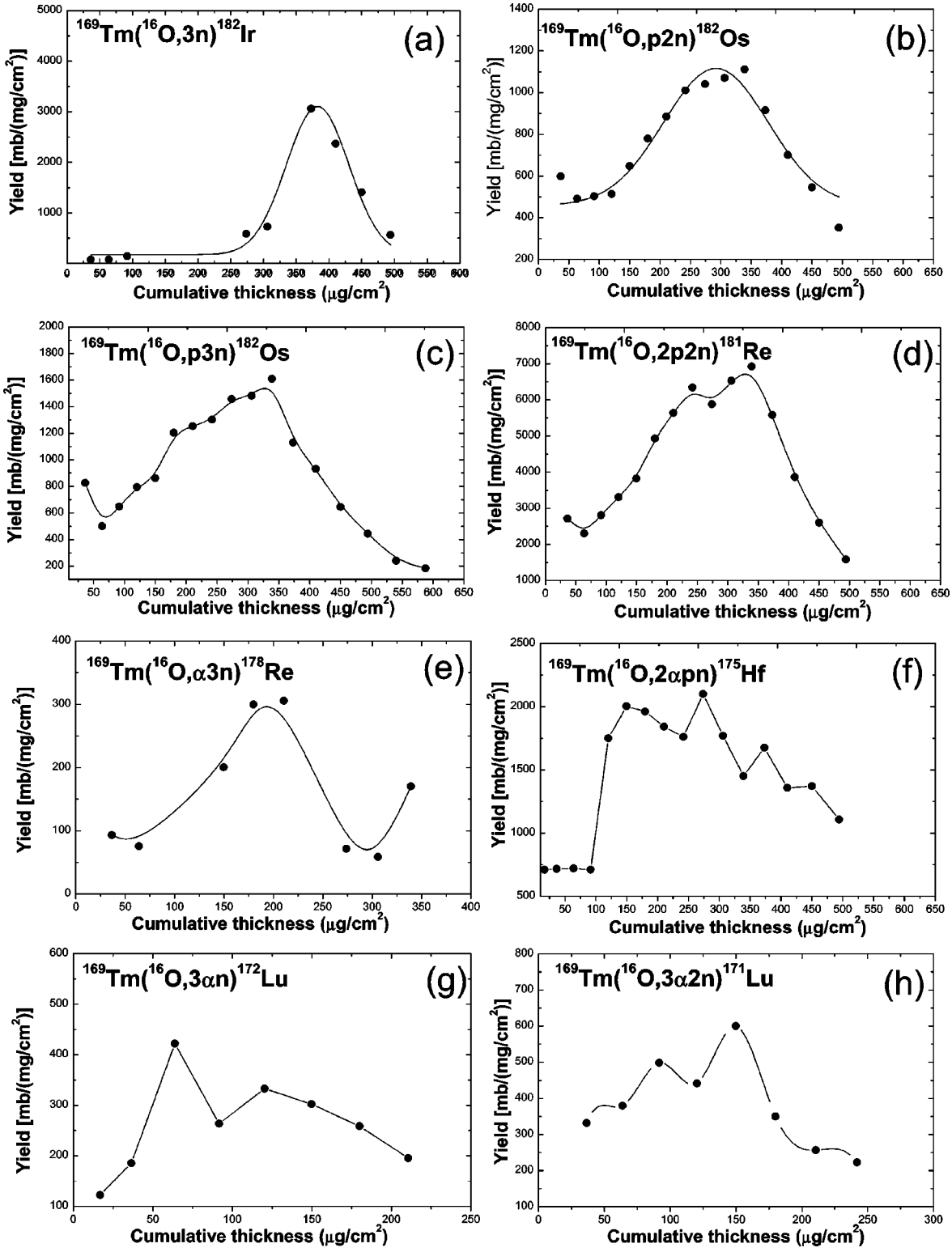

FIG. 5. The experimentally measured recoil range distributions for various radioactive residues produced in the interaction of an ^{16}O beam with a ^{169}Tm target at ≈87 MeV.

^{169}Tm(^{16}O,3αn)^{172}Lu and ^{169}Tm(^{16}O,3α2n)^{171}Lu, the measured RRDs [Figs. 5(g) and 5(h)] show two peaks at relatively lower values of cumulative catcher thicknesses at ≈75 μg/cm^2 and ≈150 μg/cm^2, respectively. This indicates that these products are not populated by the complete fusion process but by some other process in which the linear momentum transferred is less than that for complete fusion process. This is possible when only a part of the projectile

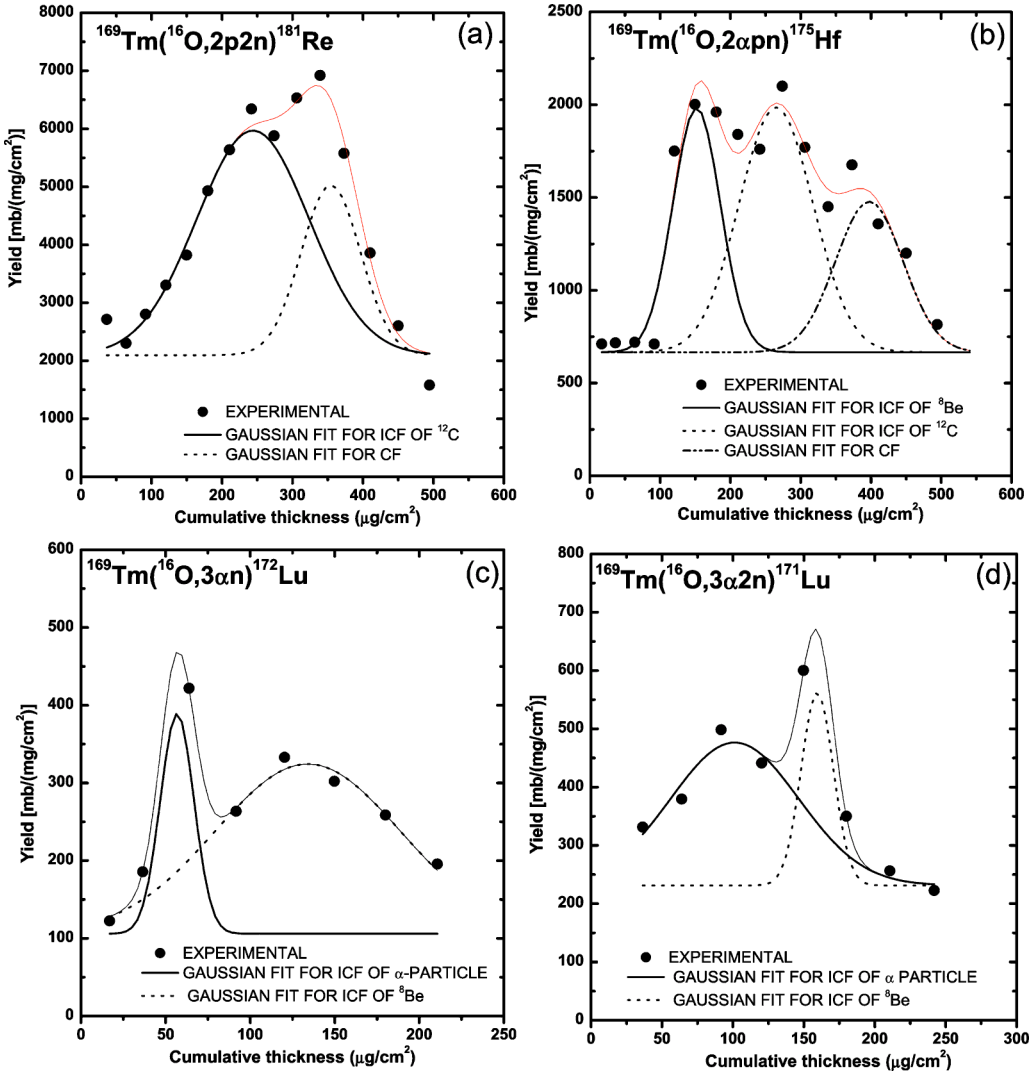

FIG. 6. (Color online) The recoil range distributions fitted with Gaussian peaks for determining the relative contributions of complete and incomplete fusion.

fuses with the target (incomplete fusion) and the rest of it moves with a velocity nearly equal to the velocity of the projectile. As such, in these reactions the contribution of complete fusion is expected to be negligible. This may also be confirmed from the fact that the theoretical calculations of EFs for these channels using all of the three codes ALICE-91, CASCADE, and PACE2 give negligible cross-sections, as has already been mentioned in the text.

In order to separate out the relative contributions of complete and incomplete fusion in the ^{169}Tm(^{16}O,$2p2n$)^{181}Re reaction, the experimentally measured RRD has been fitted with Gaussian peaks using the software ORIGIN as shown in Fig. 6(a), and the areas under the two peaks have been computed. The peak represented by dark solid curve gives the ICF contribution while the dotted curve represents the CF contribution. The relative contributions of the CF and ICF processes are obtained by dividing the area of the corresponding peak by the total area. The incomplete fusion (ICF) contribution in this case is found to be 65% and the CF contribution is about 35%, with an uncertainty of ≈5%. For the reaction ^{169}Tm(^{16}O,$2\alpha pn$)^{175}Hf, the experimentally measured RRD has been fitted with three Gaussian peaks at cumulative thicknesses ≈150 μg/cm^2, ≈260 μg/cm^2, and ≈370 μg/cm^2 as shown in Fig. 6(b). The relative contributions of CF, ICF for the fusion of fragment ^{12}C and the ICF contribution corresponding to the fusion of ^{8}Be are found to be ≈25%, ≈46%, and ≈29%, respectively, for this channel. Similarly, the relative contributions of ICF, as indicated in Figs. 6(c) and 6(d), of α-particle and ^{8}Be have been found to be ≈20% and ≈80% for the residue ^{172}Lu while ≈74% and ≈26% for the residue ^{171}Lu, respectively.

V. CONCLUSIONS

Excitation functions for eight reactions in the ^{16}O + ^{169}Tm system have been measured. Theoretical calculations based on three different computer codes with a suitable choice of the various parameters agree well with the experimental data, in general. The pre-cursor-decay has been found

to have significant contribution for $p2n$ and $p3n$ channels. The pre-cursor decay contribution has been obtained for the reaction ^{169}Tm(^{16}O,$p2n$)^{182}Os. The enhancement of experimentally measured cross sections for alpha emission channels over their theoretical predictions have been attributed to the fact that these residues are not only formed by the complete fusion but also through incomplete fusion. The RRDs for eight residues produced in the ^{16}O+^{169}Tm system have also been measured. The analysis of RRD has clearly indicated the significant contribution of ICF. An attempt has been made to obtain the relative contribution of CF and ICF channels from the analysis of the measured RRD distributions.

ACKNOWLEDGMENTS

The authors are thankful to the Director, NSC, New Delhi for extending the facilities for carrying out the experiment. We are also thankful to Dr. R. K. Bhaumik, Mr. Subir Nath for all their support during the experiment. One of the authors (M.K.S.) thanks Dr. A. K. Sinha, Director, IUC-DAEF, Calcutta Centre, Kolkata, for providing financial support and to Dr. Sandeep S. Ghugre for discussions. We also thank the Chairman, Department of Physics, AMU for providing all the necessary facilities.

[1] P. Vergani, E. Gadioli, E. Vaciago, E. Fabrici, E. Gadioli Erba, M Galmarini, G. Ciavola, and C. Marchetta, Phys. Rev. C **48**, 1815 (1993).
[2] M. Crippa, E. Gadioli, P. Vergani, G. Ciavola, C. Marchetta, and M. Bonardi, Z. Phys. A **350**, 121 (1994).
[3] B. S. Tomar, A. Goswami, G. K. Gubbi, A. V. R. Reddy, S. B. Manohar, B. John, and S. K. Kataria, Phys. Rev. C **58**, 3478 (1998).
[4] B. B. Kumar, A. Sharma, S. Mukherjee, S. Chakrabarty, P. K. Pujari, B. S. Tomar, A. Goswami, S. B. Manohar, and S. K. Dutta, Phys. Rev. C **59**, 2923 (1999).
[5] S. Chakrborty, B. S. Tomar, A. Goswami, S. K. Gubbi, S. B. Manohar, A. Sharma, B. B. Kumar, and S. Mukherjee, Nucl. Phys. **A678**, 355 (2000).
[6] S. Gupta, B. P. Singh, M. M. Musthafa, H. D. Bhardwaj, and R. Prasad, Phys. Rev. C **61**, 064613 (2000).
[7] S. Gupta, B. P. Singh, M. M. Musthafa, H. D. Bhardwaj, M. K. Sharma, R. Prasad, and A. K. Sinha, J. Phys. Soc. Jpn. **71**, 2434 (2002).
[8] M. Kumar Sharma, B. P. Singh, Sunita Gupta, M. M. Musthafa, H. D. Bhardwaj, R. Prasad, and A. K. Sinha, J. Phys. Soc. Jpn. **72**, 1917 (2003).
[9] M. K. Sharma, Ph.D. thesis, Aligarh Muslim University, Aligarh, India, 2002.
[10] S. Gupta, Ph.D. thesis, Aligarh Muslim University, Aligarh, India, 2002.
[11] M. Blann, NEA Data Bank, Report No. PSR-146, Gif-sur-Yvette, France, 1991.
[12] F. Puhlhofer, Nucl. Phys. **A280**, 267 (1977).
[13] A. Garvon, Phys. Rev. C **21**, 230 (1980).
[14] FREEDOM, Data acquisition and analysis system designed to support the accelerator based experiments at the Nuclear Science Centre, New Delhi, India.
[15] M. Cavinato, E. Fabrici, E. Gadioli, E. Gadioli Erba, P. Vergani, M. Crippa, G. Colombo, I. Redaelli, and M. Ripamonti, Phys. Rev. C **52**, 2577 (1995).
[16] E. Browne and R. B. Firestone, *Table of Radioactive Isotopes* (Wiley, New York, 1986).
[17] V. F. Weisskopf and D. H. Ewing, Phys. Rev. **57**, 472 (1940).
[18] M. Blann, Phys. Rev. Lett. **27**, 337 (1971).
[19] D. Bodansky, Annu. Rev. Nucl. Sci. **12**, 79 (1962).
[20] W. Hauser and H. Feshbach, Phys. Rev. **87**, 336 (1952).
[21] F. D. Becchetti and G. W. Greenlees, Phys. Rev. **182**, 1190 (1969).
[22] G. R. Satchler, Nucl. Phys. **70**, 177 (1965).
[23] L. C. Northcliffe and R. F. Schilling, At. Data Nucl. Data Tables **A7**, 264 (1970).